

# Influence of Carbon Nanotube Aspect Ratio on Normal Stress Differences in Isotactic Polypropylene Nanocomposite Melts

Dong-Hua Xu and Zhi-Gang Wang\*

CAS Key Laboratory of Engineering Plastics, Joint Laboratory of Polymer Science and Materials, Beijing National Laboratory for Molecular Sciences, Institute of Chemistry, Chinese Academy of Sciences, Beijing, 100080, P. R. China

Jack F. Douglas

Polymers Division, National Institute of Standards and Technology, Gaithersburg, Maryland 20899

Received September 28, 2007; Revised Manuscript Received November 26, 2007

**ABSTRACT:** We consider the impact of varying the aspect ratio  $A$  of carbon nanotubes (CNT) on the rheological properties of isotactic polypropylene/CNT nanocomposites. Specifically, we focus on multiwall CNT having a relatively *low aspect ratio* ( $A$  in the range from 22 to 45), since previous work (Kharchenko et al., *Nature Mater.* **2004**) has emphasized the rheological properties of relatively *high aspect ratio* multiwall CNT nanocomposites ( $A$  from 300 to 400). Correspondingly, we find that the formation of a *nonequilibrium* CNT network structure occurs at a higher CNT concentration in our low  $A$  CNT nanocomposites, as theoretically expected. The proposed mechanism for the large apparent negative normal stress differences ( $\Delta N$ ) described by Kharchenko et al. relies on the capacity of the “struts” of the CNT network to rotate about their impingement junctions, much like the links of a deformed chain link fence. This model implies the absence of appreciable negative  $\Delta N$  at low CNT concentrations where the network does not yet exist and also for short CNT and at high concentrations of CNT where the mesh size of the network becomes too small to accommodate appreciable rotational distortion. In conformity with this simple mechanical model, we observe only a *positive* apparent  $\Delta N$  in our CNT/iPP nanocomposites, even well above the CNT gelation concentration. This striking change in the rheology of CNT nanocomposites with a change in  $A$  has been further confirmed in die-swell measurements, where a large die swell has been seen in the short CNT nanocomposites, rather than the die-shrinkage found before for the large  $A$  or the highly “entangled” CNT network counterpart.

## Introduction

Carbon nanotubes (CNT) are promising additives for polymer materials due to their extraordinary mechanical, electrical, and thermal properties.<sup>1–3</sup> The viscoelastic properties of CNT/polymer “nanocomposites” have drawn a lot of attention due to their scientific importance as a probe of the composite dynamics and microstructure and their practical applications relating to composite processing.<sup>4–10</sup> Most previous studies have focused on the rheological and electrical conductivity properties of CNT nanocomposites. The rheological percolation thresholds, where these materials acquire the rheological characteristics of a gel and become relatively highly conductive, respectively, have been found to depend on nanotube dispersion,<sup>4</sup> aspect ratio,<sup>11</sup> CNT alignment,<sup>12</sup> and temperature.<sup>13</sup>

One of the most impressive observations for these CNT/polymer composites was the finding of large negative normal stress differences ( $\Delta N$ ) for CNT/iPP melts under steady shear flow and the corresponding observation of die-shrinkage rather than die-swelling when these materials were extruded from a pipe.<sup>7</sup> Even though negative apparent  $\Delta N$  were observed earlier in both single-wall<sup>14</sup> and multiwall<sup>15</sup> CNT dispersions in low viscosity solvents, the magnitudes of  $\Delta N$  in the solution measurements were smaller than the values found in CNT/iPP melts by orders of magnitude. The measurements on the CNT suspensions also exhibited large finite-size effects. For example, vorticity alignment was only seen under conditions where the confinement scale was comparable to the average CNT length

in solution. It is also notable that  $\Delta N$  values found in these entangled polymer melts without the CNT additive are quite large and *positive* so that the reversal of sign in these normal stress differences with the addition of CNT is all the more striking.

The negative  $\Delta N$  in the solution measurements were interpreted in terms of liquid-crystalline ordering<sup>14</sup> and an attempt was thus made to correlate these observations with the vorticity alignment<sup>15</sup> of single-wall and multiwall CNT. Large-scale and local deformation of the nanotubes was also emphasized,<sup>7</sup> but the specific mechanism responsible for the emergence of negative  $\Delta N$  (defined below) in these dispersions was not established in this pioneering work.

Kharchenko et al.<sup>7</sup> proposed a qualitative, but specific, physical model (see Figure 1) of the origin of the negative  $\Delta N$  in the polymer nanocomposites that forms the basis of the present investigation. In particular, they tentatively proposed that the fibrous “struts” of the macroscopically connected CNT network *rotate* about their impingement junction points and that the CNT *bend* rather than *extend*, much like the links of a deformed chain link fence (a cartoon of this structural model is shown in Figure 1). Since the CNT network components are much stiffer than the polymer chains, the deformed interpenetrating CNT network within the viscous polymer matrix dominates the low-frequency viscoelastic response of the nanocomposite. This simple model, which leads to a number of testable predictions, provides a framework for interpreting measurements aimed at interpreting normal stress measurements in these nanocomposites. For example, this model implies the *absence* of negative  $\Delta N$  for low CNT concentration nanocom-

\* Corresponding author. E-mail: zgwang@iccas.ac.cn.

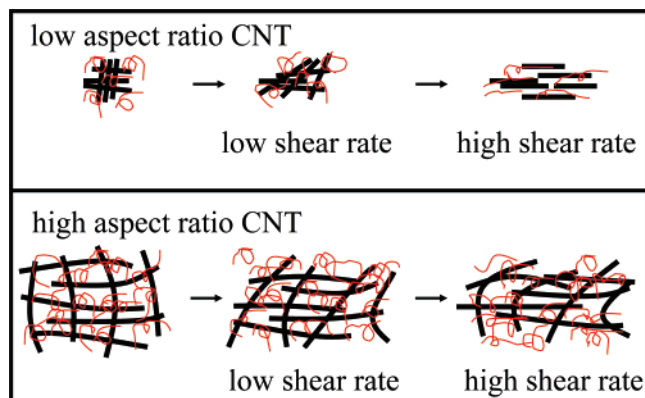


**Figure 1.** Models about deformations of low aspect ratio CNT/iPP and high aspect ratio CNT/iPP networks under steady shear.

posite since there is then no CNT network. The model also indicates that  $\Delta N$  will not be negative for sufficiently short CNT since the mesh size of the CNT network will at some point become too small to accommodate appreciable rotational distortion. This physical picture also leads us to expect that negative  $\Delta N$  should disappear at sufficiently high CNT concentrations for the same reason. Other factors, such as the polydispersities of the CNT length and diameter and the thermodynamic interactions between the CNT, are also implicated by this model to play important roles in the negative  $\Delta N$  effect since these factors, along with the entangling nature of the polymers that links the CNT network to the polymer matrix, can be expected to affect the formation and stability of the jammed CNT network. The physical problem under discussion is evidently of significant complexity, so we confine ourselves to the relatively simple problem of whether the negative  $\Delta N$  effect indeed disappears for low aspect ratio CNT, as the conceptual model of Kharchenko et al.<sup>7</sup> would suggest.

We point out that even the origin of positive  $\Delta N$  in entangled polymer melts is an incompletely understood phenomenon from a molecular perspective, although the Doi–Edwards reptation model provides some insight.<sup>16</sup> This effect means that shearing a viscoelastic material between parallel plates leads to a thrust on the plates that drives them apart. Normal stresses also reveal themselves in everyday activities with complex fluids. The rod-climbing commonly observed when stirring paint and other viscous fluids derives from positive  $\Delta N$ .<sup>17</sup> The swelling of viscous materials upon extrusion such as the children's toy Play-Doh<sup>18</sup> is also characteristic of materials with positive  $\Delta N$ . Negative normal stresses are exciting because we can expect these common flow patterns to be turned “upside down” so that an extruded material would be expected to shrink rather than swell when extruded, which is exactly what Kharchenko et al.<sup>7</sup> observed in their high aspect ratio CNT nanocomposite extrusion measurements. Following up on the work of Kharchenko et al.,<sup>7</sup> we investigate whether the use of low aspect ratio CNT leads to die swelling instead of die-shrinkage, as the conceptual model of Kharchenko et al. further suggests.

## Experimental Section

**Preparation and Characterization of Chemically Modified Multiwall CNT.** To enhance the dispersion of CNT in iPP, commercially available multiwall CNT (CVD method, Shenzhen Nanotech Port Co., China)<sup>18</sup> were chemically modified as follows. The CNTs were purified and converted into a functionalized acid form [CNT(COOH)<sub>n</sub>] via sonication in a 1:3 relative volume fraction nitric acid–sulfuric acid mixture at 40 °C. The resultant solid was then washed with deionized water until the pH was 6 and then an excess NaOH solution was added until the pH value

became near 14, converting CNT(COOH)<sub>n</sub> into a sodium salt, [CNT(COONa)<sub>n</sub>]. The CNT(COONa)<sub>n</sub> nanotubes were recovered by centrifuging at 3000 rpm (1 rpm = 2π radians per min in SI units) for 10 min and the resultant solid was washed with deionized water until the pH value was again 6. Cetyltrimethylammonium bromide (CTAB), C<sub>18</sub>H<sub>37</sub>Br, CNT(COONa)<sub>n</sub>, and water were mixed and the suspension was continuously refluxed under vigorous stirring for 12 h. When the stirring was stopped, the suspension separated into a clear, colorless top solution with a black precipitate on the container bottom. The precipitate was collected and placed in a Soxhlet extractor. Deionized water (200 mL) was added over a period of 24 h to extract the remaining CTAB, followed by the addition of chloroform (200 mL) for another 24 h to remove the remaining C<sub>18</sub>H<sub>37</sub>Br. The solid material from the Soxhlet extractor was dissolved in chloroform at a mass fraction concentration of 1%. The solution was put in a sonication bath for 2 h and centrifuged at 3000 rpm for 10 min. The upper solution was collected and distilled to obtain the resultant solid. Finally, the solid material, the alkyl-modified CNT, CNT(COOC<sub>18</sub>H<sub>37</sub>)<sub>n</sub>, was dried under vacuum at room temperature.<sup>19</sup>

The aspect ratio of the CNT(COOC<sub>18</sub>H<sub>37</sub>)<sub>n</sub> nanotubes was measured by using scanning electron microscopy (SEM, Hitachi S-4300, Japan). A dilute CNT(COOC<sub>18</sub>H<sub>37</sub>)<sub>n</sub> chloroform solution was deposited onto a clean aluminum foil to form a thin film after the chloroform evaporation and the film was then subjected to examination by SEM. We obtained CNT(COOC<sub>18</sub>H<sub>37</sub>)<sub>n</sub> nanotube length distribution data from these SEM observations.

**Preparation of CNT/iPP.** The iPP sample employed in this work was a commercial product of Aldrich Chemical Co. (relative molecular masses  $M_w = 340\,000$  and  $M_n = 97\,000$  and melt index of 4.0). The iPP sample of 3.4 g was added into 110 mL of xylene in a flask, and this flask was put into an oil bath under nitrogen atmosphere at a temperature of 130 °C. After the iPP had dissolved for 20 min, the oil bath temperature was then set to 120 °C and the iPP solution was then stirred for 1 h before dispersing the CNT-(COOC<sub>18</sub>H<sub>37</sub>)<sub>n</sub> in the iPP solution. This 0.25% mass fraction CNT-(COOC<sub>18</sub>H<sub>37</sub>)<sub>n</sub> dispersion was sonicated for 2 h to break up the CNT clusters. We added this xylene dispersion of CNT(COOC<sub>18</sub>H<sub>37</sub>)<sub>n</sub> to the iPP solution to yield a prescribed mass ratio of CNT-(COOC<sub>18</sub>H<sub>37</sub>)<sub>n</sub> to iPP. We continuously stirred this mixture for another 1.5 h and then mixed it with a large quantity of methanol having a relative mixture/methanol volume ratio of 1 to 7. The precipitate of CNT(COOC<sub>18</sub>H<sub>37</sub>)<sub>n</sub>/iPP was washed with methanol 3 times and then put in ventilator for 48 h to evaporate the solvent. The recovered sample was dried at 60 °C under vacuum for 3 days. Eight samples were prepared by using the same procedure where the relative mass concentration of CNT(COOC<sub>18</sub>H<sub>37</sub>)<sub>n</sub> was equal: 0%, 0.2%, 0.5%, 1.0%, 2.0%, 3.8%, 7.4%, and 9.1%, respectively. The nanocomposites made of CNT(COOC<sub>18</sub>H<sub>37</sub>)<sub>n</sub> and iPP are indicated as X% mass fraction CNT/iPP below, where X% represents the CNT concentration.

**Rheological Measurements.** Rheological measurements were performed on a stress-controlled rheometer AR2000 (TA Instruments Ltd.) equipped with parallel-plate geometry (diameter of 25 mm) under a nitrogen atmosphere. The samples for rheological measurement were prepared by pressing the CNT/iPP material at 200 °C into disks with a thickness of 1 mm and diameter of 25 mm in a stainless steel die. In the rotary rheometer measurements, the samples were initially squeezed in place before the actual measurements began (the impact of this procedure on the observed nanocomposite rheology is discussed below). We first melted the samples at 210 °C for 5 min in the rheometer and then compressed them to 1000 μm. With the sample edge scraped, the samples were then compressed a distance of 50 μm at a rate of 100 μm/s while the temperature was increased up to 210 °C. We adopted this procedure in order to have the samples to conform to the gap distance of our apparatus (950 μm) and to ensure sufficient contact between the nanocomposite samples and the rheometer plates. Experimental conditions are as follows: Thermal history effects were reduced by holding the samples in the rheometer at an elevated temperature (210 °C) for 10 min prior to running tests. Oscillatory

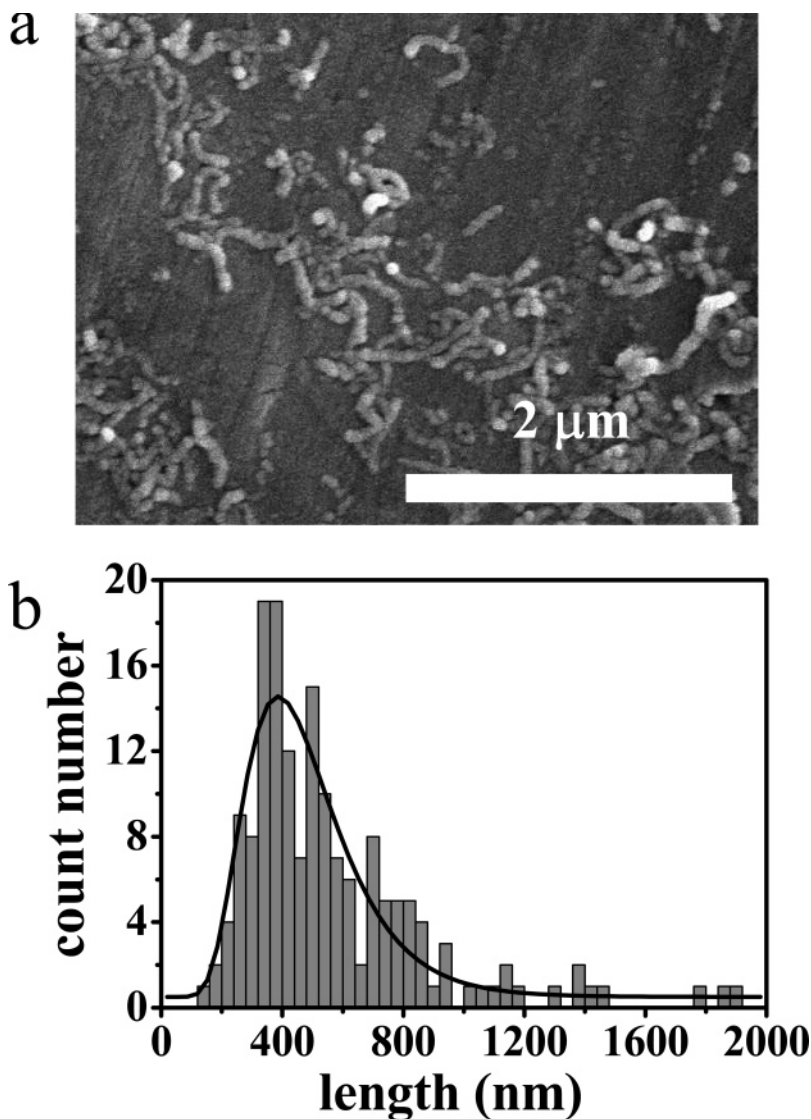


**Figure 2.** SEM image of CNT(COOC<sub>18</sub>H<sub>37</sub>)<sub>n</sub> (a) and corresponding length distribution of CNT(COOC<sub>18</sub>H<sub>37</sub>)<sub>n</sub> (b).

frequency sweeps from 100 to 0.1 rad/s were then carried out, where we selected a strain amplitude of 2% to be within the linear viscoelastic regime. After these oscillatory frequency sweeps, the samples were then melted in the rheometer at 210 °C for 10 min to help erase the strain history. Then steady shear measurements were performed at the same temperature with shear rate in the range between 0.00125 and 10 s<sup>-1</sup>. The relative uncertainty associated with the rheometer measurements is 0.5%.

To examine whether there was any die contraction for CNT/iPP nanocomposites with a CNT concentration higher than the critical CNT gelation concentration (see below), a CNT/iPP sample having a 7.4% mass fraction was examined by melt extrusion. A pure iPP sample was also extruded for comparison purpose. The extrusion was performed at 210 °C on a Rosand RH7 capillary rheometer (Bohlin Instruments Ltd., UK). A capillary die with diameter of 1 mm and length to diameter-ratio (L/D) of 32 was used. Extrudates at different plunger speeds (i.e., different shear rates) were then collected for the die contraction examination without any post-drawing.

## Results and Discussion

### CNT Characterization and CNT Gelation Concentration.

The CNT gelation concentration for CNT/iPP is known to depend on CNT aspect ratio.<sup>20</sup> To estimate aspect ratios of the chemically modified CNT, we laboriously estimated the size

of the CNT by direct SEM observation. A typical SEM image of CNT is shown in Figure 2a. The length distribution of the CNT is obtained through image analysis and the result is shown in Figure 2b. In Figure 2b, a lognormal distribution function was used to fit the length histograms of the CNT, the average length of the CNT and the standard uncertainty were gotten from the fitting results. The average length of the CNT is found to be 447 ± 2 nm (here and below ± represents the standard relative uncertainty unless otherwise indicated). The observational uncertainty of the measurement of the length of CNT was ±1%. Our estimate of the diameter of the CNT is especially uncertain since the CNT were coated with gold to perform the SEM measurements, which led to larger apparent CNT diameters in Figure 2a than their true values. The mean diameter estimated in this way was found to be about 75 nm ± 1 nm. The observational relative uncertainty of the measurement of the diameter of CNT was less than 2%. Given this large deviation, we instead take the diameters of the original CNT (10 to 20 nm) provided by the producer to estimate the aspect ratios of our CNT. This leads to an aspect ratio *A* estimate of the CNT in the range of 22 to 45. In ref 7, the aspect ratios of CNT were reported to be in the range between 300 and 400, corresponding to a CNT gelation concentration near a 1% volume fraction or about a 2% mass fraction. Because the CNT

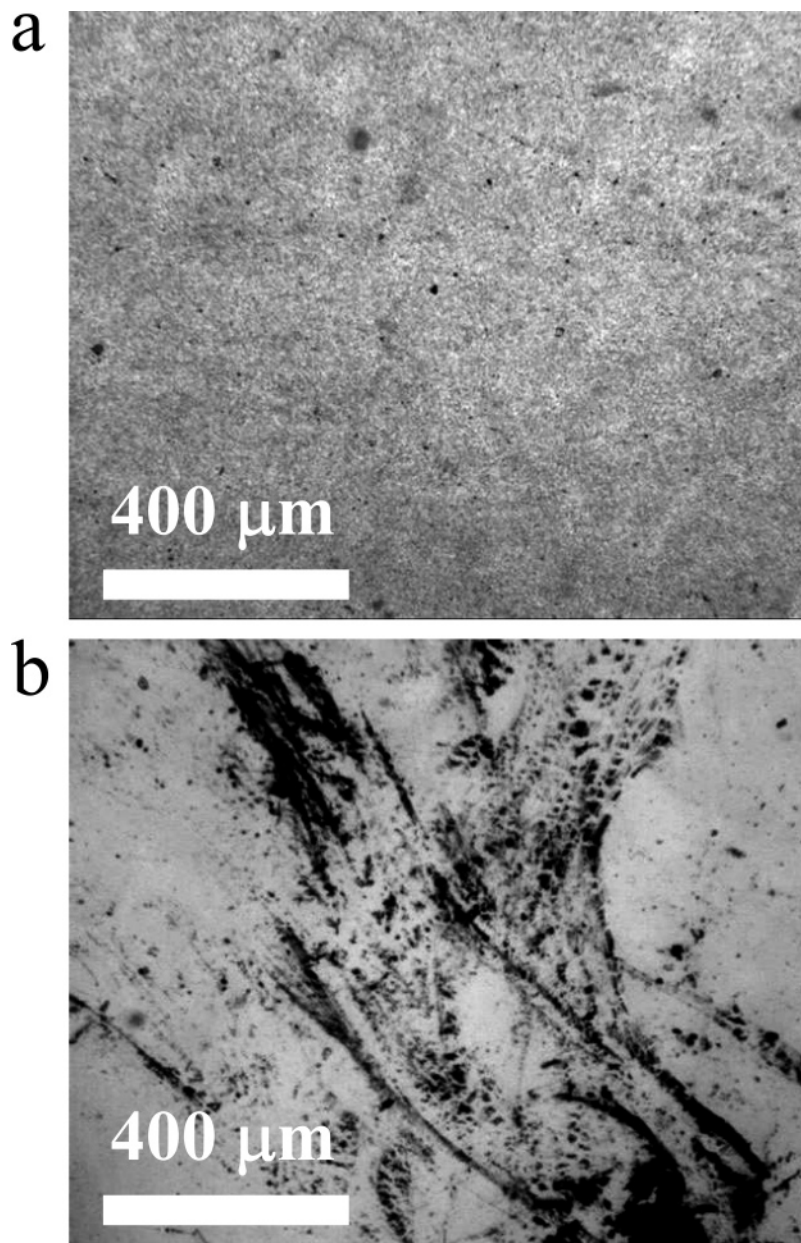


**Figure 3.** Optical micrographs of CNT/iPP nanocomposites at 200 °C in the bright field. CNT(COOC<sub>18</sub>H<sub>37</sub>)<sub>n</sub> nanocomposite (a) and pristine CNT nanocomposite (b) with a CNT concentration of 1.0% mass fraction.

used in our study have much lower aspect ratios, the CNT/iPP are naturally expected to have a much higher CNT gelation concentration, as we confirm below.

The average length of our CNT is about 450 nm (Figure 2b) or about 0.5 μm so that the CNT length of these tubes is about an order of magnitude smaller than those used in ref 7. The nanotube diameter in the earlier work was predominantly in the range between 20 and 25 nm<sup>3,21</sup> and the length of CNT was estimated to be between 6 and 10 μm. On the basis of these rough estimates, ref 7 reported the aspect ratio *A* of their CNT to be in the range from 300 to 400 after melt blending. They also estimated *A* to be close to 1000 before melt mixing, which makes it apparent that the history of the mixing process can appreciably affect the CNT length in polymer nanocomposites. While there is considerable uncertainty in the exact value of the average aspect ratio for these CNT materials, which is a general problem for all CNT materials, the aspect ratio of our nanotubes is about an order of magnitude smaller than those considered by Kharchenko et al.,<sup>7</sup> and this difference should

allow a test of their conceptual model of the origin of the negative normal stress effect in CNT composites.

An appraisal of the dispersion of CNT in the polymer matrix is an important element in any nanocomposite structure–property study. To evaluate this dispersion, optical micrographs of CNT/iPP at the molten state were collected. An optical microscope (Carl Zeiss JENA, Germany) equipped with a CCD camera (HV1301UC, made by Da Heng Company, Beijing) was used here to observe the CNT dispersion in the molten state of the CNT/iPP at 200 °C. The optical micrograph of 1.0% mass fraction CNT/iPP at 200 °C in Figure 3a shows that the CNT are relatively uniformly distributed in iPP at a μm length scale. Although there are some diffuse aggregates of the CNT, these aggregates occupy only a small portion of the CNT nanocomposite material. Overall, the CNT are considered to be reasonably “well dispersed” in the iPP, at least at scales accessible by optical microscopy. This relatively good dispersion of the CNT in iPP is facilitated by interactions between iPP chains and the grafted alkyl chains on the surfaces of CNT. It should be pointed

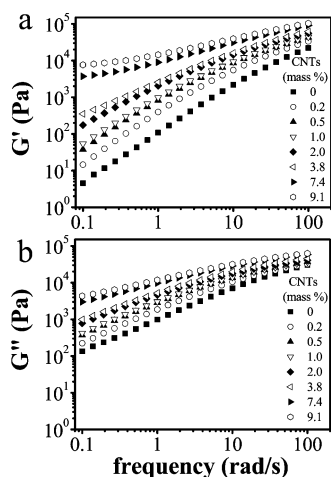


**Figure 4.** Storage modulus  $G'$  (a) and loss modulus  $G''$  (b) of CNT/iPP vs frequency at 210 °C.

out that the chemical modification on CNT is necessary to achieve good dispersion in such short CNT nanocomposites, as can be easily confirmed by the relatively poor dispersion found when mixing our pristine CNT into iPP under equivalent conditions as blending the functionalized CNT (see Figure 3b).

**Linear Viscoelastic Characterization of CNT Nanocomposite Melts.** The dispersion of the CNT in a polymer matrix has a large impact on the rheology of these dispersions and thus has a large influence on the processing of these materials. These changes in rheological properties, in turn, can provide some insight into the structural properties of the CNT/iPP. Figure 4 shows the frequency sweep curves for storage modulus,  $G'$ , (Figure 4a) and loss modulus,  $G''$ , (Figure 4b), of our CNT/iPP nanocomposites at 210 °C. Evidently, the CNT have a dramatic effect on the rheological properties of these composites, an effect similar to previous observations on the highly entangled CNT composites. Both  $G'$  and  $G''$  increase with increasing CNT concentration, especially at low frequencies. For CNT/iPP with CNT concentration of 7.4% mass fraction, we see that  $G'$  seems to reach a plateau value at low frequencies, which indicates an occurrence of a transition from the liquidlike to gellike viscoelastic behavior.<sup>5,8</sup> The absence of relaxation behavior at low frequencies is attributed to the formation of a CNT network.<sup>7</sup> For a CNT/iPP nanocomposite having an even higher CNT concentration of 9.1% mass fraction, the gellike viscoelastic response becomes even more pronounced, as evidenced by increased magnitude of the nanocomposite modulus. At high frequencies, the polymer relaxation apparently dominates the stress relaxation, while at low frequencies the CNT network dominates the viscoelastic response. The polymer nanocomposite is thus an interpenetrating network composed of a CNT network and an entangled polymer matrix, which has its own network structure.

The frequency dependence of loss tangent ( $\tan \delta$ ) is depicted in Figure 5. For materials near the liquid-to-solid transition,  $\tan \delta$  should decrease with increasing frequency in the pregel regime for a typical viscoelastic liquid. In the post-gel regime, we see that a moderate increase in  $\tan \delta$  appears with increasing frequency, indicating the elastic character of these materials.<sup>22,23</sup>

For our CNT/iPP,  $\tan \delta$  begins to increase with frequency at low frequencies for a CNT concentration near a 7.4% mass fraction, which is a rheological symptom of physical gelation. We thus identify this concentration roughly with the CNT gelation concentration in our nanocomposite material. This critical concentration is much larger than the value found in ref 7, where the CNT gelation concentration was found to be about

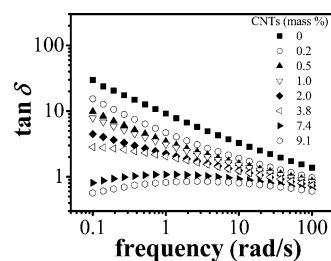


**Figure 5.** Loss tangent ( $\tan \delta$ ) of CNT/iPP vs frequency at 210 °C.

1% by volume fraction or 2% by mass fraction. A qualitative change in the gelation concentration of this kind is expected. For example, Bicerano et al.<sup>20</sup> indicate that the random close packing (dispersion gelation) concentration for rodlike particles having an  $A$  near 60 should be about a 14% volume fraction, while rods having an aspect ratio of about 400 should have CNT gelation volume fraction near a 3% volume fraction. The polydispersity of rodlike particles can be expected to lower these critical concentrations somewhat so that the observed values of the critical gelation concentration in the present work and that in ref 7 are in reasonable agreement with the estimates by Bicerano et al.<sup>20</sup>

**Nonlinear Viscoelastic Characterization of CNT Nanocomposite Melts.** Previous work has demonstrated that the rheological properties of CNT/iPP nanocomposites are sensitive to steady shear flow. In Figure 6a, we show the viscosity of the CNT/iPP melt dispersion under steady shear. Evidently, when the CNT concentrations (7.4% and 9.1% mass fractions) are above the gelation concentration, the CNT/iPP exhibit appreciable shear thinning at relatively low shear rates, as found and discussed previously by Kharchenko et al.<sup>7</sup> This shear thinning behavior is contrasted with the nearly constant viscosity found in this range of shear rates for CNT/iPP mixtures for concentrations lower than a 7.4% mass fraction. (Of course, even the pure polymer melt exhibits shear thinning at higher shear rates due to the influence of shear on the entangled polymer melt.) Shear thinning similar to that exhibited in Figure 6a has been reported in other extended nanoparticle filled polymer materials such as using nanoclay<sup>24</sup> and nanofiber additives,<sup>25</sup> due to the effects that we associate with the breakdown of the nanoparticle network, as well as the nanoparticle shape distortion and particle orientation with respect to the applied shear field.

The observation of appreciable shear thinning in a material exhibiting elastic behavior in the limit of small deformation rates implies the existence of a yield stress.<sup>26</sup> The presence of a yield stress  $\tau_y$  in our samples is suggested by the sharp drop in the shear viscosity at low shear rates in Figure 6a for CNT concentrations higher than a 7.4% mass fraction, although it is difficult to make viscosity measurements at low enough shear rates to resolve the shear rate at which a transition from an elastic response to viscous flow response occurs. We make a tentative estimate of the yield stress by directly examining the shear stress as a function shear rate in Figures 6b to 6e. In particular, we estimate  $\tau_y$  values to be about 730 Pa (Figure 6d) and 1200 Pa (Figure 6e) for the 7.4% and 9.1% CNT mass fractions samples, respectively, but only shear thinning is evident in the samples that were not initially in a CNT network gel state. Although the estimates are highly uncertain, the apparent yield stress seems to increase with increasing CNT mass fraction, which is what we should generally expect from the enhanced elasticity at higher CNT concentrations. The yield stress can thus be attributed to the existence of a CNT network structure within the polymer matrix that resists breaking until

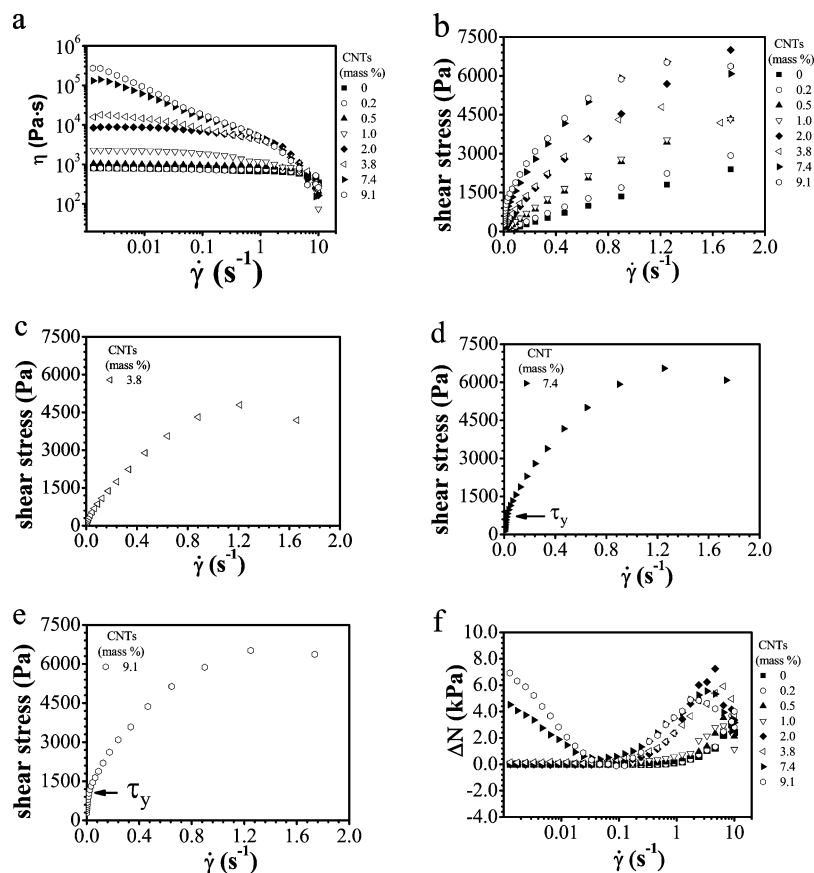


**Figure 6.** Steady shear viscosity ( $\eta$ ) of CNT/iPP (a), shear stress of CNT/iPP (b), shear stress of 3.8% mass fraction CNT/iPP (c), shear stress of 7.4% mass fraction CNT/iPP (d), shear stress of 9.1% mass fraction CNT/iPP (e), and normal stress differences ( $\Delta N$ ) of CNT/iPP (f), vs shear rate at 210 °C. The abrupt drop of the apparent viscosity at low shear rates in (a) at concentrations in the CNT gel regime is symptomatic of yield, although it is difficult to go to low enough shear rates to resolve the yield transition with high accuracy.

the applied stress exceeds  $\tau_y$ . This yielding phenomenon could be very important in applications such a fire suppression where the structural integrity of the network under fluid flow is key to the beneficial effect of the CNT additive to the polymer matrix.<sup>27</sup>

We next compare with Kharchenko's observations on normal stress differences for CNT/iPP under steady shear. In the case of a parallel-plate geometry, the measured normal force is actually the difference of the normal stress differences,  $\Delta N = N_1 - N_2$  (the normal stress differences  $N_1$  and  $N_2$  are defined as  $(\tau_{11} - \tau_{22})$  and  $(\tau_{22} - \tau_{33})$ , respectively, where  $\tau_{ii}$  are the normal stresses acting along the flow (1), flow gradient (2), and vorticity (3) directions).<sup>7</sup> In Figure 6f, we show our observations for the normal stress differences observed for our CNT dispersion at 210 °C. At low shear rates,  $\Delta N$  are nearly zero for our nanocomposites with CNT concentrations less than 7.4% mass fraction, while they become large in magnitude and *positive* for the samples beyond gelation concentration. The above obvious difference between the "unentangled" and "entangled" (CNT concentrations above the gelation value) nanocomposites arises from the normal forces induced by squeezing the high CNT concentration CNT/iPP nanocomposite. Evidently, the "resting time" of 10 min after squeezing is not sufficient to allow complete relaxation of the normal forces for the gellike samples of 7.4% and 9.1% mass fraction CNT/iPP.

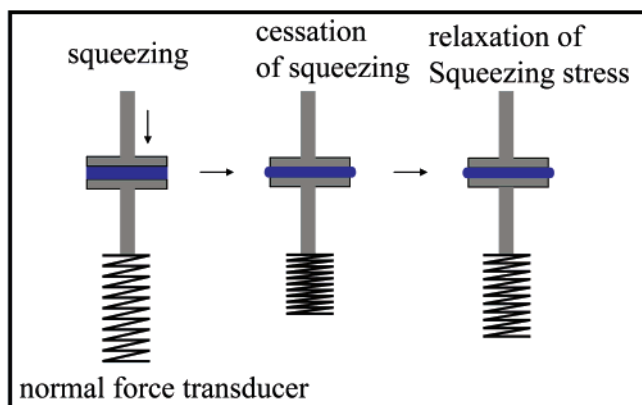
Note that the instrumental compliance might contribute somewhat to the observed initial normal stress differences,<sup>28,29</sup> especially given the highly elastic nature of the composite due to nanotube reinforcement. Although we plan to investigate this effect further in future measurements, especially for nanocom-

posite samples containing relatively long CNT where the elastic effects are exceptionally large, we expect this contribution to the apparent normal stress measurements to be minor in our current measurements since we have chosen the large plate gap width (about 950  $\mu\text{m}$ ) in the observations.<sup>30</sup> In addition, if we compare the normal stress differences among all the samples we investigated at different gap widths and under similar experimental conditions, our observations agree to within reasonable measurement uncertainties so there is little sensitivity to the chosen gap width. We conclude that the large  $\Delta N$  values that we see for the gellike 7.4% and 9.1% mass fraction CNT/iPP samples mainly reflect the contribution of the gel rather than the instrument. In a later section, we will show that the initial normal stress differences at low shear rates for the gellike samples of 7.4% and 9.1% mass fraction CNT/iPP can be decreased by controlling the compression conditions, which further indicates that the contribution of instrument compliance can be basically neglected for the purposes of this article.

We also observed in Figure 6f that the  $\Delta N$  of the gellike samples show minima at low shear rates near  $0.07 \text{ s}^{-1}$ . In high-density polyethylene (HDPE) melts, a similar phenomenon has sometimes been observed and attributed to a sign change in the first normal stress differences.<sup>31</sup> However, this interpretation is debatable, and more observations and modeling are still needed to reliably interpret this singular rheological feature. We next offer our own tentative interpretation to this phenomenon.

Given the gellike interpenetrating network nature of the CNT nanocomposites, we can expect the weakly entangled CNT network (due to the relatively short length of the CNT) to be distorted under flow. This distortion naturally leads to a

a



b

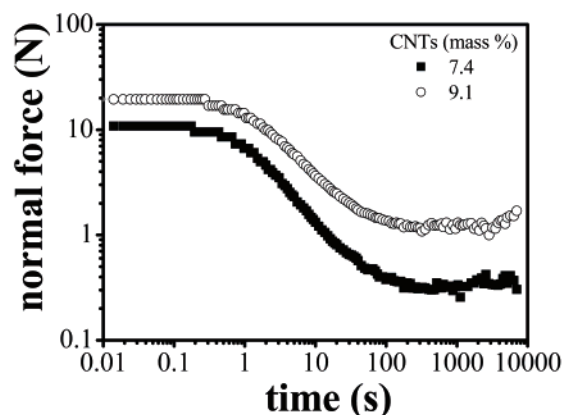


**Figure 7.** Schematic of squeezing flow induced by compressing the nanocomposite between two parallel plates in TA AR2000 rheometer (a) and the decay of normal force with time after a squeezing flow of 7.4% and 9.1% mass fractions CNT/iPP at 210 °C. The compression rate was 100  $\mu\text{m/s}$  and the total deformation was 50  $\mu\text{m}$  (b).

reduction of the normal stress differences as in previous measurements, but at very high shear rates, the network can be expected to break down under flow so that the CNTs begin to align along the flow direction (see Figure 1). The loss of the network integrity should then give rise to a sharp increase in  $\Delta N$  arising from the elastic entangled polymer matrix contribution to  $\Delta N$ . The apparent minima in the normal stress differences for the low  $A$  CNT/iPP melts suggest that the CNT network may give rise to a compensating negative  $\Delta N$  contribution, but that the large positive  $\Delta N$  contributions arising from the entangled polymer melt and the disruptive effect of shear flow on the CNT network limit the extent of the CNT contribution to the net value of  $\Delta N$  for the nanocomposites. We will address this initial decrease of the normal stress differences at low shear rates in next section.

**Relaxation after a “Squeezing” Deformation.** In all rotary rheometer measurements, the samples are initially squeezed in place before the measurements are initiated, and we schematically illustrate this squeezing deformation in Figure 7a for our TA AR2000 rheometer. After the edge of the sample is scraped off of excess material, the test material is then subjected to a compressive deformation or “squeezing”. When the set-point gap height of the instrument is reached, the squeezing then stops. After cessation of deformation, the stress induced by squeezing should relax, but the question is how much time does this relaxation process require? The spring in Figure 7a represents

a normal force transducer that allows us to follow the evolution of this “squeezing stress” in time. To quantify this relaxation process, we then performed zero shear stress creep experiments to record the value of squeezing stress with normal force transducer.<sup>32,33</sup> Figure 7b shows the decay of the squeezing stress (represented by the normal force) with time in a log–log plot for CNT/iPP with relatively high CNT concentrations (7.4% and 9.1% CNT mass fractions). It is evident from Figure 7b that the squeezing stress exhibits a rather rapid initial elastic relaxation after cessation of the squeezing deformation, and then it remains relatively *constant* afterward. This stress plateau persists even after 2 h, which means that the nanocomposite is more like a solidlike paste or gel<sup>33</sup> than a fluid proper in its viscoelastic response. The absence of complete normal stress relaxation after a cessation of squeezing deformation is a consequence of the CNT network within the composite, which *traps residual stresses* in the network. Evidently, there is not enough time for the normal stresses to relax on the timescales of our rheological experiments and it is not clear if relaxation will occur after *any* reasonable amount of time given that the material is in a *nonequilibrium “jammed” state*. While further experimental results showed that waiting for longer times does not lead to a substantial reduction of squeezing stress associated with sample preparation, there are other ways to assess the influence of the squeezing step on the apparent rheological properties of CNT/iPP nanocomposites.

The purpose of the squeezing step is to ensure sufficient contacts between the samples and plates, but the squeezing stress induced by the deformation of the stiff CNT network may be difficult to relax so that deformation can be plastic rather than viscous. Therefore, the following procedure was used to enhance contact between the nanocomposite samples and plates, while minimizing the squeezing stress as much as we could. We start with the same 7.4% mass fraction CNT/iPP nanocomposite sample utilized in the measurements described above. We designate this sample as test sample 2 (T2) to distinguish it from the original test sample (T1). We first melted the T2 sample at 210 °C for 5 min in the rheometer and then compressed it to a gap distance of 1100  $\mu\text{m}$  where the rate of compression was set at 10  $\mu\text{m/s}$ . The sample was then allowed to relax until the squeezing stress was less than 50 Pa for every 10  $\mu\text{m}$  compression. After the gap reached 1000  $\mu\text{m}$ , the sample edge was again scraped of excess material. When the oven temperature increased to 210 °C, the sample was compressed until the gap distance reached 980  $\mu\text{m}$  using the same compression procedure. Oscillatory frequency sweep and steady shear experiments were performed, respectively, as in the first test of the sample. In Figure 8a, we see that  $\tan \delta$  of the T2 sample shows a moderate increase with increasing frequency in the low-frequency region, indicating that the material is highly elastic. This behavior is essentially the same as the observation on the 7.4% mass fraction CNT/iPP sample without the stress-reduction treatment of the T2 sample preparation. While this observation is reassuring regarding the effect of sample preparation on the rheological measurements, Figure 8b indicates that the change of  $\Delta N$  with shear rate in the T2 sample exhibits a trend different from that of the T1 sample at low shear rates. In particular,  $\Delta N$  of the T2 sample *does not* exhibit the decrease at low shear rates found for the T1 sample, although a similar trend is found for the T1 and T2 samples at shear rates above 0.1  $\text{s}^{-1}$ . According to these observations, residual stress effects associated with sample preparation can evidently have an appreciable influence on the apparent value of  $\Delta N$ , especially at low shear rates. This behavior is not an artifact, but rather is intrinsic to

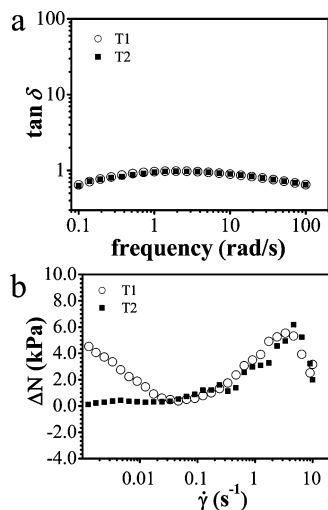


**Figure 8.** Loss tangent ( $\tan \delta$ ) of the CNT/iPP nanocomposite sample upon first testing (T1 sample) and the second testing (T2 sample). Sample conditions: 7.4% mass fraction CNT/iPP vs frequency at 210 °C (a) and normal stress differences ( $\Delta N$ ) of the T1 and T2 samples vs shear rate at 210 °C. The height of gap was 950  $\mu\text{m}$  and 980  $\mu\text{m}$ , respectively (b).

the nonequilibrium nature of these materials. The material properties depend on deformation history and these properties can be locked or “switched” by controlling processing. This plasticity of material properties is a headache from a materials characterization standpoint, but these memory effects offer potential advantages for the functioning of these complex materials if they can be controlled.

**Influence of CNT Aspect Ratio on Normal Stress Differences Observations.** Since normal stress measurements are generally plagued by a host of difficulties that can compromise these measurements and since nonequilibrium characteristics are prevalent in these pastelike materials, we performed extrusion experiments to characterize how these materials *qualitatively* flow. Normal stress differences are well-known to have a dramatic effect on extrusion and other free boundary fluid flows,<sup>34</sup> and we can then expect to gain basic insight into the nature of the effective normal stresses in these materials by observing the flow of these materials. Figure 9 provides some illustrative images of some extrudates obtained from a capillary rheometer for a pure iPP melt and 7.4% mass fraction CNT/iPP nanocomposite melt at relatively high shear rates ( $> 100 \text{ s}^{-1}$ ). Evidently, die swell occurs after extrusion for both the pure iPP and the CNT/iPP nanocomposite samples which is expected phenomenon for fluids with an appreciable positive  $\Delta N$ .<sup>35</sup> Notably, the extent of die swell in the nanocomposite is smaller than that in the pure iPP. This can probably be attributed to the CNT network within the iPP matrix, which results in stress transfer from iPP matrix to the CNT network, thereby retarding the elastic recovery of the iPP chains.<sup>36</sup> We find that the diameter expansion factor in these measurements ranges from 1.18 to 1.66 when the 7.4% mass fraction CNT/iPP is extruded with shear rate varying from 100 to 2000  $\text{s}^{-1}$ , while the corresponding diameter expansion factor ranges from 1.34 to 1.82 (The relative uncertainty of the diameter expansion factor is taken to be equal the relative uncertainty estimate of extrudate diameter which we determine to be about 1%) when the pure iPP is extruded within the same shear rate range. We infer that the effective value of  $\Delta N$  and the die swell both remain positive in our CNT/iPP nanocomposite melts under these shear flow conditions, but notably the die swell is reduced in magnitude relative to the pure iPP melt. These observations are contrasted

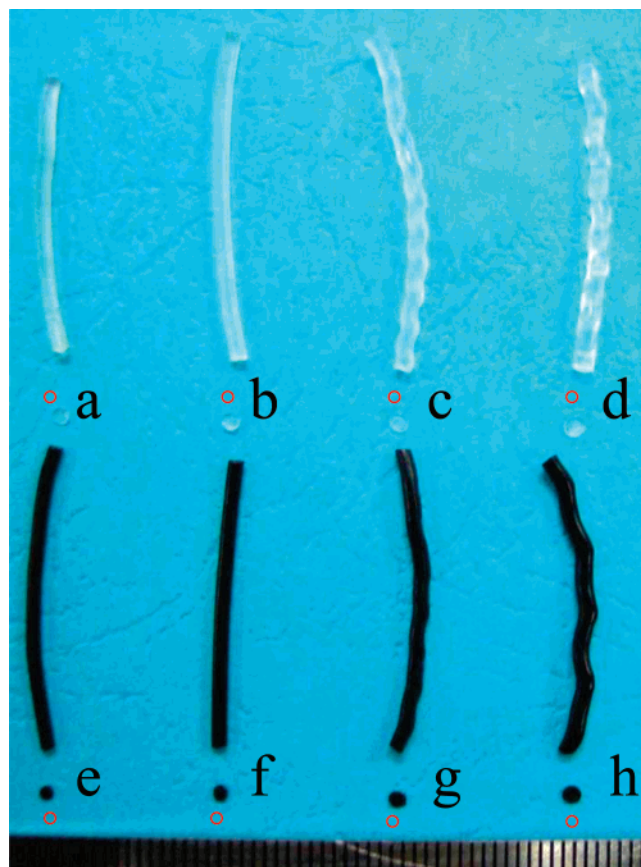


**Figure 9.** Photos of extrudates of pure iPP and CNT/iPP melt (7.4% mass fraction) at 210 °C under different shear rates. The diameter and length of capillary die were 1 and 32 mm, respectively. iPP at 100  $\text{s}^{-1}$ , mean diameter of 1.34 mm (a), iPP at 500  $\text{s}^{-1}$ , mean diameter of 1.46 mm (b), iPP at 1000  $\text{s}^{-1}$ , mean diameter of 1.67 mm (c), iPP at 2000  $\text{s}^{-1}$ , mean diameter of 1.82 mm (d), 7.4% mass fraction CNT/iPP at 100  $\text{s}^{-1}$ , mean diameter of 1.18 mm (e), 7.4% mass fraction CNT/iPP at 500  $\text{s}^{-1}$ , mean diameter of 1.38 mm (f), 7.4% mass fraction CNT/iPP at 1000  $\text{s}^{-1}$ , mean diameter of 1.54 mm (g), 7.4% mass fraction CNT/iPP at 2000  $\text{s}^{-1}$ , mean diameter of 1.66 mm (h). The red circle in the figure shows the size of the capillary die for comparison. The minimum scale of the ruler at the downside of the figure is 1 mm. The relative measurement uncertainty of the extrudate diameter was estimated to be about 1%.

with those of ref 7 where CNT/iPP extrudates having a 2.5% volume fraction and a high aspect ratio CNT exhibited large negative apparent  $\Delta N$  under shear conditions and where the extrudate diameter correspondingly actually *shrank* by an impressive factor of 0.77 upon extrusion. The shape-distortion instability of the extrudate was also examined for both the pure iPP and 7.4% mass fraction CNT/iPP nanocomposite. Shape-distortion in our measurements was also reduced, but the effect we observed is much smaller in magnitude than the effect found in the measurements of Kharchenko et al.<sup>7</sup> Both sets of measurements thus appear to be internally consistent between the viscoelastic and pipe flow measurements. At any rate, we conclude that our low aspect ratio nanocomposites exhibit a radically different flow rheology from the highly entangled CNT nanocomposites considered by Kharchenko et al.<sup>7</sup>

**Quantifying CNT Deformability under Flow.** Next, we consider the propensity of the CNT to deform under flow. Yu et al. measured the deformation of comparable multiwall CNT.<sup>37</sup> The Young's modulus  $E_Y$  was estimated to be 40 GPa and the bending stiffness  $S$  was about  $1.22 \times 10^{-20} \text{ N m}^2$  for CNT.<sup>37</sup> The “stiffness parameter”  $S$  can be estimated as

$$S = E_Y \pi d^4 / 2^6 \quad (1)$$

where the dimensionless bending stiffness equals  $S/(\eta\dot{\gamma}L^4)$  and the dimensionless “bending ratio” is  $E_Y[\ln(r_e) - 1.5]d^4/(2\eta_0\dot{\gamma}L^4)$ , where  $r_e = 1.24r_p/\sqrt{\ln r_p}$  and  $r_p = L/d$ . The dimensionless bending ratio ranges are estimated to vary in the range between  $O(10^2)$  to  $O(10^4)$  for  $\dot{\gamma}_0$  of  $0.001 \text{ s}^{-1}$  and between  $O(10^{-2})$  and  $O(10^0)$  for  $\dot{\gamma}_m$  of  $10 \text{ s}^{-1}$  when the CNT concentration decreases from 9.1% to 0.2% mass fraction. A dimensionless bending ratio less than unity indicates a tendency toward fiber bending, so that the short CNT used in our study can deform at a high shear rate. In contrast, if we take  $\eta_0$  on the order of  $O(10^5)$ , as suggested in ref 7, the dimensionless bending ratio in ref 7 ranges from  $O(10^{-2})$  to  $O(10^{-6})$  as shear rate increases from 0.001 to  $10 \text{ s}^{-1}$ , indicating that the large  $A$  CNT nanotubes considered in ref 7 should readily bend under flow.

Even under conditions where no network exists, recent simulations have indicated that the propensity of the fibers to bend under flow in solution can contribute to the observation of negative normal stresses. For example, Becker et al. simulated the flow-induced deformation of a high-aspect-ratio elastic filament.<sup>38</sup> For a dilute, statistically homogeneous suspension of elastic filaments, he found shear thinning and positive first normal stress differences at relative low flow rates, but he also found negative  $\Delta N$  at high flow rates even in this simple model. The main point learned from these idealized computations is that the coupling between the fluid motion and the deformation of the fibers under flow can lead to the emergence of negative  $\Delta N$ .

**Working Model for Normal Stress Differences Observations.** The modeling of Becker et al. does not address itself to the existence of a CNT network within the polymer matrix, which seems to be essential for the observation of appreciable negative normal stress differences in the polymer nanocomposite melt. Kharchenko et al.<sup>7</sup> went on to argue physically that the stiff mesh structure in their highly entangled CNT network becomes distorted under shear flow in such a manner that the CNT network structure tilts due to the inextensible nature of the network struts and the freely jointed “hinges” of the impinging junctions that define the CNT network. In particular, it was suggested that this should lead to a reduction of the average network mesh size along the shear gradient direction and a corresponding increase of the average mesh size along the flow direction as the cellular structures of the network become “squashed” by the deformation of the network. (Imagine shearing the top of a chain link fence in the plane of the fence or shearing the cell structure of an open-celled foam structure having stiff, but deformable cells where a similar tilting of the cell mesh should arise.) This picture is contrasted with the one presented by Jamney et al.<sup>39</sup> in an attempt to explain the origin of negative normal stress differences in deformed semiflexible biopolymer gels (see Figure 3 of Jamney et al.),<sup>39</sup> where filament stretching was suggested to be responsible for the negative  $\Delta N$  phenomenon in the biopolymer network. We do not think that filament stretching can be appreciable in the CNT network, and we would be surprised if this were the case for the fibers in the biopolymer network exhibiting negative  $\Delta N$  as well.

Kharchenko et al. conceived the negative  $\Delta N$  to arise through network cell rotation process under flow and the absence of appreciable CNT extension under deformation was implicit in this model. The distorted CNT network is then taken to exert a retractive force on the normal shearing surfaces of the rheometer, where this interaction is mediated through the polymer matrix.<sup>7</sup>

Although we do not observe negative  $\Delta N$  in our low aspect ratio CNT nanocomposite melts, recent simulations by Rodney

et al.<sup>40</sup> provide some insight in this change in rheological behavior with CNT aspect ratio. Rodney et al. examine the critical conditions that define the formation of semiflexible fiber entanglement networks in a simple computational model that does not incorporate hydrodynamic interactions, which is a reasonable model if the elastic interactions are strongly dominated by the fibers. These simulations show a *qualitative change* in the elasticity of these networks when the semiflexible fibers become short [ $A \sim O(10)$ ] so that the fibers no longer effectively bend.<sup>40</sup> Theoretically, the concentration scaling of the shear modulus of stiff entangled fiber networks is predicted to qualitatively change upon going from long to short fibers and this theoretical finding provides additional evidence to a significant change in the elasticity of networks composed of long vs short semiflexible fibers. (Note that the critical fiber packing density or gelation concentration estimates of Rodney et al.<sup>40</sup> match up reasonably well with our CNT nanocomposite measurements.) It thus seems that the deformability of the individual CNT and the CNT network are implicated in the observed negative  $\Delta N$ .

**Quantifying CNT Network Entanglement.** We note that even the high  $A$  nanotube networks break down under shear if the CNT concentration is just above the CNT gelation threshold, which makes the properties of the CNT nanocomposite melts highly susceptible to flow perturbation.<sup>41</sup> In contrast, Alig et al.<sup>42</sup> found that the CNT network within the nanocomposite (CNT/iPP) retained its integrity for a CNT concentration well above the gelation concentration. It is a general experience that the CNT networks are more robust to flow perturbation when the CNT concentration is high.<sup>42</sup>

We can obtain some further insight into the CNT entanglement in CNT/iPP nanocomposites by quantifying the average mesh size of the CNT network. For a CNT network, we estimate the network mesh size  $\xi$  by the proposed relation<sup>43</sup>

$$\xi = d \sqrt{3/2\phi} \quad (2)$$

where  $d$  is the diameter of CNT and  $\phi$  the volume fraction (eq 2 ignores the deformation of network shape under flow). This estimate of  $\xi$  indicates a CNT mesh size of 62 to 124 nm for our entangled 7.4% mass fraction CNT/iPP nanocomposite, while we estimate  $\xi$  to be much larger (between 245 and 306 nm) for the corresponding entangled CNT/iPP nanocomposite at a 1% CNT volume fraction in ref 7. (The standard uncertainty of our mesh size estimate should be comparable to the standard uncertainty of the diameter of CNT. However, since the diameter of CNT can only be roughly estimated we cannot reliably calculate the standard uncertainty of mesh size at this time.) We conclude the mesh size of the high  $A$  nanotube composites is roughly a factor of 2–5 times larger than the mesh scale in the low  $A$  nanocomposite, a trend similar to the relative size ratio of the CNT in these two systems. We can take the ratio of the CNT length to the mesh size as measure of the extent of topological interaction strength in the network, the larger this ratio the greater the entanglement. In ref 7, the length of CNT is 20–40 times of the mesh size of the CNT network of a 1% volume fraction CNT/iPP nanocomposite and accordingly, we define the topological interaction strength  $T$  to be in the range between  $T = 20$  and  $T = 40$ . Similarly, the average length of our short CNT is 4 to 8 times of the mesh size of the CNT network of our 7.4% mass fraction CNT/iPP nanocomposite, indicating a  $T$  value in the range between 4 and 8. In ref 7, if the CNT concentration is also 7.4% mass fraction (3.9% volume fraction), the mesh size of CNT network will be between 123 and 154 nm and  $T$  value will then range between 40 and 80.

Evidently, the entanglement intensity, as measured by  $T$ , is much lower in our CNT network than that of ref 7, rationalizing how the high aspect ratio CNT network can endure larger deformation than the low aspect ratio CNT network without structural failure.

We now return to the cartoon of the CNT network in Figure 1 to describe our view of the deformation of the high and low aspect ratio CNT networks in light of the topological interaction strength responsible for network formation. The low aspect ratio nanotube network has fewer topological interaction regions (“entanglements”) of CNT than the high aspect ratio nanotube network. At low shear rates, though the number of CNT entanglements decreases with increasing shear rate, the iPP chains between nanotubes can bridge isolated nanotubes. This means that low aspect ratio nanotube network can only sustain its form at small deformation. Thus, a small deformation of CNT network is not expected to produce sufficient negative  $\Delta N$  in CNT/iPP composites. With a further increase in shear rate, the low aspect ratio CNT network can be destroyed completely and the nanotubes then align along shear flow direction,<sup>15</sup> leaving a large positive normal stress effect from the elastic deformation of the polymer melt. For the high aspect ratio CNT network, it then becomes more difficult to disentangle the network through flow. While CNT entanglements may be destroyed when the nanotubes rotate,<sup>43</sup> new entanglements form as the CNT collide with each other during shear.<sup>44</sup> The formation of entanglements of this kind has only been observed for long multiwall CNT, but this type of network has been studied for a long time in systems of fibers.<sup>45</sup> This phenomenon is absent for short multiwall CNT measurements in ref 39. Increasing the length of the CNT thus enhances the stability and formation of the nonequilibrium entanglement network in polydisperse CNT composites rather generally.

## Conclusions

The rheological properties of low aspect ratio CNT/iPP nanocomposites are contrasted with the observations of Kharchenko et al.<sup>7</sup> for high aspect ratio CNT in isotactic polypropylene. We find that the aspect ratio of CNT has a strong influence on the CNT gelation concentration, which is perhaps more reassuring than surprising. On the other hand, this is an extremely practical result. It is important to know that the viscoelastic flow properties under nonlinear flow conditions of these nanocomposites can be so strikingly different. For the low aspect ratio CNT/iPP nanocomposites, the apparent  $\Delta N$  are observed to be strictly positive, although we do observe an initial decrease with increasing shear rate, followed by an increase again at high shear rates. These observations are contrasted with the high aspect ratio CNT composite measurements where large *negative* apparent  $\Delta N$  were reported. (We use the term *apparent* given the nonequilibrium nature of the nanocomposite material.) This dramatic change in flow rheology was also confirmed by looking at the extrusion of CNT nanocomposite melts from an orifice, where the low aspect ratio composite exhibited *die swell* and where the high aspect ratio CNT composite exhibited *die shrinkage*. These observations are in line with the observations of apparent normal stress differences of opposite signs in these CNT nanocomposite materials.

We elaborate on a physical model of these striking normal stress effects that was introduced before by Kharchenko et al.<sup>7</sup> This model is based on the view that the negative normal stresses derive from a (rotational) deformation of the CNT network within the polymer matrix where the CNT are considered to be flexible, but essentially inextensible. The existence of negative

normal stress differences within this model requires for the entanglement network to remain stable under deformation. This condition is shown to be met in the experiments on high aspect ratio CNT by Kharchenko et al., but this is apparently *not* the case in our measurements on our low aspect ratio CNT nanocomposites. Thus, the negative normal stress effect should not be present or should be much diminished in magnitude in low aspect ratio CNT networks relative to the highly entangled high aspect ratio CNT networks. We quantify the extent of entanglement to better understand this change in rheology.

This model of normal stress effect changes in the CNT composites also implies a change from negative  $\Delta N$  to positive  $\Delta N$  under certain well-prescribed conditions. For example, the network should no longer be able to retain its integrity at low CNT concentrations and at shear rates high enough for the CNT within the network to align appreciably with the flow. At very high CNT concentrations, the long CNT must become highly entangled, but the mesh size of these rigid fibers should become correspondingly small, approaching ultimately a scale on the order of the average CNT diameter. When this happens, it is hard to image how the network mesh units can rotate without some extension of the fiber elements. Since the CNT are quite inextensible, we expect the negative  $\Delta N$  to *change sign* at high CNT concentrations for high aspect ratio CNT. The negative  $\Delta N$  effect is then predicted to occur for CNT long enough and at a sufficient concentration to form a compliant entanglement network that is stable over large-scale deformation under flow.

We note that the low aspect ratio CNT used in our experiments have been chemically (alkyl-) modified to enhance dispersion, while the CNT considered in ref 7 were not modified in this way. While this chemical modification could influence the stability of the CNT network somewhat, we do not expect this modification to change the qualitative differences that we see between the large and small aspect ratio CNT samples. To gain a better understanding of the surface functionalization effect, we plan to investigate the effect of dispersion of unmodified CNT into other polymer matrices where the mechanical dispersion of the short tubes seems to be possible, such as polylactide polymers. We also plan to study the influence of the polymer molecular mass since this variable can be expected to influence the coupling of the CNT network to the polymer matrix through polymer–CNT entanglement interactions and tuning of the normal stress contributions from the polymer melt matrix. It will be interesting to see how surface functionalization and the molecular characteristics of the polymer matrix (monomer chemistry as well as entanglement interactions) influence the normal stress properties of this novel class of nanocomposites.

**Acknowledgment.** Z.-G.W. expresses thanks for financial support from “One Hundred Young Talents” Program of Chinese Academy of Sciences, National Science Foundation of China with Grant No. 10590355 for the Key Project on Evolution of Structure and Morphology during Polymer Processing and National Science Foundation of China with Grant No. 20674092. We thank Dr. Kharchenko (Masco Corporation, Taylor, MI) for valuable comments on our paper.

## Appendix

Since the CNT used in the study are relatively short, it is worth examining whether CNT Brownian motion or fluid inertia plays any significant role. The Péclet number (ratio of the shear rate to the rate of particle reorientation due to the Brownian motion) and the Reynolds number (ratio of the inertial energy

to viscous dissipation energy) are calculated. The Péclet number,  $Pe$ , can be estimated from the CNT rotary diffusion coefficient by  $Pe = \dot{\gamma}/D_r$ , where  $\dot{\gamma}$  is the shear rate, and  $D_r$  the rotary diffusion coefficient. For dilute rods,  $D_r$  is defined by eq 3:<sup>46</sup>

$$D_r = D_0 = 3k_B T [\ln(L/d) - 0.8] / (\pi \eta L^3) \quad (3)$$

In the semidilute regime, it has been argued that excluded-volume interactions lead to a modification of  $D_r$ <sup>16</sup>

$$D_r = \beta D_0 (nL^3)^{-2} = \beta D_0 [(4/\pi) \phi (L/d)^2]^{-2} \quad (4)$$

that can then be used to calculate an effective  $Pe$ . In the above equations,  $k_B$  is the Boltzmann constant,  $T$  the temperature,  $L$  the nanotube length (the average length of 447 nm),  $d$  the nanotube diameter (10 to 20 nm),  $\eta$  the shear viscosity,  $\beta$  a constant ( $\approx 1350$ ),<sup>47</sup>  $n$  the number density of nanotubes, and  $\phi$  the volume fraction of nanotubes.  $\phi$  can be obtained from mass fraction of CNT, with the densities of CNT<sup>13</sup> and iPP of 1.75 and 0.9 g/cm<sup>3</sup>, respectively. The Reynolds number is estimated as

$$Re \approx \dot{\gamma} h^2 \rho / \eta \quad (5)$$

where  $\rho$  is the mass density of iPP and  $h$  the gap between two parallel plates. Thus, the Péclet number in CNT/iPP in this study is so huge ( $Pe \approx 10^5$  to  $10^{12}$ ) that Brownian motion is negligible, while the Reynolds number is terribly small ( $Re \approx 10^{-10}$  to  $10^{-5}$ ). In ref 7, the Péclet number and the Reynolds number were  $O(10^{14}-10^{16})$  and  $O(10^{-11}-10^{-8})$ , respectively, so the situation is basically similar for these two basic measures of fluid flow rate.

## References and Notes

- Koerner, H.; Price, G.; Pearce, N. A.; Alexander, M.; Vaia, R. A. *Nat. Mater.* **2004**, *3*, 115–120.
- Ramasubramaniam, R.; Chen, J.; Liu, H. *Appl. Phys. Lett.* **2003**, *83*, 2928–2930.
- Kashiwagi, T.; Grulke, E.; Hilding, J.; Groth, K.; Harris, R.; Butler, K.; Shields, J.; Kharchenko, S.; Douglas, J. *Polymer* **2004**, *45*, 4227–4239.
- Mitchell, C. A.; Bahr, J. L.; Arepalli, S.; Tour, J. M.; Krishnamoorti, R. *Macromolecules* **2002**, *35*, 8825–8830.
- Pötschke, P.; Fornes, T. D.; Paul, D. R. *Polymer* **2002**, *43*, 3247–3255.
- Meincke, O.; Kaempfer, D.; Weickmann, H.; Friedrich, C.; Vathauer, M.; Warth, H. *Polymer* **2004**, *45*, 739–748.
- Kharchenko, S. B.; Douglas, J. F.; Obrzut, J.; Grulke, E. A.; Migler, K. B. *Nat. Mater.* **2004**, *3*, 564–568.
- Du, F.; Scogna, R. C.; Zhou, W.; Brand, S.; Fischer, J. E.; Winey, K. I. *Macromolecules* **2004**, *37*, 9048–9055.
- Zhang, Q.; Lippits, D. R.; Rastogi, S. *Macromolecules* **2006**, *39*, 658–666.
- Hu, G. J.; Zhao, C. G.; Zhang, S. M.; Yang, M. S.; Wang, Z. G. *Polymer* **2006**, *47*, 480–488.
- Krishnamoorti, R.; Yurekli, K. *Curr. Opin. Colloid Interface Sci.* **2001**, *6*, 464–470.
- Moniruzzaman, M.; Winey, K. I. *Macromolecules* **2006**, *39*, 5194–5205.
- Pötschke, P.; Abdel-Goad, M.; Alig, I.; Dudkin, S.; Lellinger, D. *Polymer* **2004**, *45*, 8863–8870.
- Davis, V. A.; Ericson, L. M.; Parra-Vasquez, A. N. G.; Fan, H.; Wang, Y. H.; Prieto, V.; Longoria, J. A.; Ramesh, S.; Saini, R. K.; Kittrell, C.; Billups, W. E.; Adms, W. W.; Hauge, R. H.; Smalley, R. E.; Pasquali, M. *Macromolecules* **2004**, *37*, 154–160.
- Lin-Gibson, S.; Pathak, J. A.; Grulke, E. A.; Wang, H.; Hobbie, E. K. *Phys. Rev. Lett.* **2004**, *92*, 048302.
- Doi, M.; Edwards, S. F. *The Theory of Polymer Dynamics*; Oxford University Press: New York, 1986.
- Weissenberg, K. *Nature (London)* **1947**, *159*, 310–311.
- Certain equipment, instruments, or materials are identified in this paper in order to adequately specify the experimental details. Such identification does not imply recommendation by the NIST, nor does it imply that the materials are necessarily the best available for the purpose.
- Xu, D. H.; Liu, H.; Yang, L.; Wang, Z. G. *Carbon* **2006**, *44*, 3226–3231.
- Bicerano, J.; Douglas, J. F.; Brune, D. A. *J. Macromol. Sci.—Rev. Macromol. Chem. Phys.* **1999**, *C39*, 561–642.
- Andrews, R.; Jacques, D.; Rao, A. M.; Derbyshire, F.; Qian, D.; Fan, X.; Dickey, E. C.; Chen, J. *Chem. Phys. Lett.* **1999**, *303*, 467–474.
- Liu, C. Y.; Zhang, J.; He, J. S.; Hu, G. H. *Polymer* **2003**, *44*, 7529–7532.
- Winter, H. H.; Mours, M. *Adv. Polym. Sci.* **1997**, *134*, 165–234.
- Solomon, M. J.; Almusallam, A. S.; Seefeldt, K. F.; Somwangthananroj, A.; Varadan, P. *Macromolecules* **2001**, *34*, 1864–1872.
- White, J. L.; Czarnecki, I.; Tanaka, H. *Rubber Chem. Technol.* **1980**, *53*, 823–835.
- Tsitsilianis, C.; Iliopoulos, I.; Ducouret, G. *Macromolecules* **2000**, *33*, 2936–2943.
- Kashiwagi, T.; Du, F. M.; Douglas, J. F.; Winey, K. I.; Harris, R. H.; Shields, J. R. *Nat. Mater.* **2005**, *4*, 928–933.
- Niemiec, J. M.; Pesce, J.; McKenna, G. B.; Skocypec, S.; Garritano, R. F. *J. Rheol.* **1996**, *40*, 323–334.
- Zapas, L. J.; McKenna, G. B. *J. Rheol.* **1989**, *33*, 69–91.
- Davies, G. A.; Stokes, J. R. *J. Rheol.* **2005**, *49*, 919–922.
- Hussein, I. A.; Williams, M. C. *J. Non-Newtonian Fluid Mech.* **1999**, *86*, 105–118.
- TA Instruments. *Thermal Analysis & Rheology*; RH063, Texas Instruments: Dallas, TX.
- Langelaan, H. C.; Gotsis, A. D. *J. Rheol.* **1996**, *40*, 107–129.
- Tanner, R. I. *J. Polym. Sci., Part A-2: Polym. Phys.* **1970**, *8*, 2067–2078.
- Chiu, W. Y.; Hsueh, T. C. *J. Appl. Polym. Sci.* **1986**, *32*, 4663–4678.
- Mohanty, S.; Nayak, S. K. *Mater. Sci. Eng., A* **2007**, *443*, 202–208.
- Yu, M. F.; Lourie, O.; Dyer, M. J.; Moloni, K.; Kelly, T. F.; Ruoff, R. S. *Science* **2000**, *287*, 637–640.
- Becker, L. E.; Shelley, M. J. *Phys. Rev. Lett.* **2001**, *87*, 19830.
- Janmey, P. A.; McCormick, M. E.; Rammensee, S.; Leight, J. L.; Georges, P. C.; Mackintosh, F. C. *Nat. Mater.* **2007**, *6*, 48–51.
- Rodney, D.; Fivel, M.; Dendievel, R. *Phys. Rev. Lett.* **2005**, *95*, 108004.
- Obrzut, J.; Douglas, J. F.; Kharchenko, S. B.; Migler, K. B. *Phys. Rev. B* **2007**, *76*, 195420.
- Alig, I.; Lellinger, D.; Dudkin, S. M.; Pötschke, P. *Polymer* **2007**, *48*, 1020–1029.
- Hough, L. A.; Islam, M. F.; Janmey, P. A.; Yodh, A. G. *Phys. Rev. Lett.* **2004**, *93*, 168102.
- Hobbie, E. K.; Fry, D. J. *J. Chem. Phys.* **2007**, *126*, 124907.
- Schmid, C. F.; Klingenberg, D. J. *Phys. Rev. Lett.* **2000**, *84*, 290–294.
- Larson, R. G. *The Structure and Rheology of Complex Fluids*; Oxford University Press: New York, 1999.
- Fry, D.; Langhorts, B.; Kim, H.; Grulke, E.; Wang, H.; Hobbie, E. K. *Phys. Rev. Lett.* **2005**, *95*, 038304.

MA702178E